Journal of Mines, Metals and Fuels, *71(12C): 114-124; 2023. DOI: 10.18311/jmmf/2023/47263*

Print ISSN : 0022-2755

Journal of Mines, Metals and Fuels

Contents available at: *www.informaticsjournals.com/index.php/jmmf*

Numerical Study of 2D Radiated Viscous Nanomaterial Over Unsteady Stretching Surface Under Impact of Porous Media, Ohmic Effect and Suction or Blowing

R. Sumithra[1]*, P. A. Dinesh[2], Sweeti Yadav[2], K. R. Roopa[2], Sudhir Patel[3], M. Hema[1], S. Subhash[1], S. A. Srikanth[1] and N. Rohith Raj[1]

[1]Department of Mathematics, Nrupathunga University, Bangalore - 560054, Karnataka, India; sumitradiya@yahoo.com

[2]Department of Mathematics, M S Ramaiah Institute of Technology, Bangalore - 560054, Karnataka, India; dineshdpa@msrit.edu, sweetiyadav1989@gmail.com, krroopa870@gmail.com

[3]Department of Mathematics, New Horizon College of Engineering, Bangalore - 560103, Karnataka, India

Abstract

The current study presents a numerical model of emitted viscous nanomaterial by the stretching of the surface with porous media, Ohmic effect and suction or blowing. The partial differential equation is converted into a system of basic differential equations using the appropriate technique. The RKF45 approach is used to provide a numerical solution to the resulting problem. The influence of several significant parameters on velocity values, concentration, temperature, and the Nusselt number is calculated, and demonstrations are presented using figures and tables. The results obtained are compared to those obtained earlier. The main conclusions of this study are that heat transfer rate increases with Ohmic effect and decreases with porosity and suction/blowing effect. The findings have ramifications in a variety of sectors, including nuclear reactors, synthetic fabrics, metal extrusion, and crystal formation.

Keywords: *Nanomaterials, Ohmic Effect, Suction or Blowing*

1.0 Introduction

Nanomaterials have a single particle size in the range of 1 to 100 nm. Nanoscale materials often have unique optical, electrical power, thermophysical, or physical capabilities. Metal (Al, Au, Cu, Fe, Ag), metal oxide (Al_2O_3, TiO_2, CuO), layered (Al+ Al_2O_3, Cu+C), carbon materials (graphite, CNTs, diamond) and nitride (AlN, SiN) are among the most often utilised nanomaterials. Nanomaterials are becoming more commercialised and widely used. Several academics are studying the rheology of nanofluids. Sakidis was the first to analyse the movement of water in an impermeable solid surface *vs* a limited length surface[1]. He observed that the dynamic boundary layer equation works well for as long as the boundaries of the layer conditions differ in both cases. Crane extends Sakiadis work by investigating fluid flow through a lengthened plate with velocity proportional to its displacement from the slit[2]. Since Choi coined the term, scientific research into nanofluids has developed at an exponential pace. His research shows that the heat conductance of these micro fluids improves in the manufacture and utilisation of Newtonian fluids. Buongiorno examined the critical parameters of Brownian particle diffusion and thermophoresis scattering in nanofluid transport[4]. Various researchers expanded on this work in areas

**Author for correspondence*

related to MHD, permeability surfaces, nonlinear magnetic fields, viscous dissolution the production of heat, chemical reaction, and Arrhenius radiation[5-11].

The movement of boundary layers caused by stretchable sheets occurs in many real-world scenarios. It has a variety of applications, including hot rolling, paper manufacturing, condensed procedure, manufactured fibres, and so on. The stretching surface might be either linear or complicated. Crane was the first to look into the straight stretching surface[2], whereas Khan and Pop looked into the irregular stretching surface[12]. Makinde and Aziz extend this investigation on the boundary's convective state[13]. Cortell was the very first to analyse boundary layer movement caused by an unevenly extended sheet in the form of heat emission and dissipation that is viscous[14]. Prasad *et al*., and Mukhopadhyay examined heat transfer in a non-isothermal stretched sheet[15,16]. The Arrhenius equation with an energy source were examined by Srinvasulu and Bandari using a nonlinearly expanded plate[17]. Ahmad banji Jafar, Sharidan Shafie, and Imran Ullah investigated MHD radiative nanofluid flow in a porous medium generated by a nonlinear stretching sheet[18]. This paper investigates the thermal and mass transfer of an electrically powered incompressible nanofluid technology over a hot stretched surface caused by a convective boundary wall. Elgazery examined flows in an inclined magnetic field across an irregular extended medium with a thermal source or sink[19]. Jafar *et al*., studied not linear flexible sheets in pore-filled materials[20]. Saeed *et al*., examined a tiny layer of nanofluid on an inclined stretched surface[21]. Rasool *et al*., simulated nanofluid movement with convection over a boundary condition using a nonlinear extending surface[10]. Abbas *et al*., examined the heat transmission properties and thermal loss of nanofluid mixes across porous, uneven, curve-shaped surfaces[22].

Porosity is an object attribute that describes the total amount of vacant or pore-filled spaces in a substance. A porous thing has a high capacity of retaining fluids inside self. Using porous material with lesser porosity improves convection thermal transfer. For example, Jue investigated open convection within a porous chamber with internal heat production[23]. The goal of his research was to investigate the effect of the porous material's presence on both hydrodynamic and thermal characteristics caused by wall overheating as well as to the inside heat input. The results revealed that a greater porosity rate yields a lower Nusselt coefficient value. Pavel investigated the influence of putting a metal-based porous substance within a conduit on the transfer of heat rates using computational and experimental approaches[24]. It was determined that increasing the Reynolds number of a material or reducing the degree of porosity might result in greater heat rates.

The physical action of a current passing through a conductor of electricity producing thermal energy is known as joule heating. Resistance ovens, resistance direct heating, induction heating is some of the applications of joule heating. Joule heating effect and chemical reaction effect on peristaltic transporting on couple-stress micropolar nanofluids in a narrow channel allows for electro kinetic transmission is studied by K. Venugopal Reddy[25]. The continuous flow of an incompressible a two-dimensional Oldroyd-B nanofluid across a stretched sheet is examined using Magneto-Hydrodynamics (MHD) and a medium that is porous with magnetically charged, joule effect, electrical, and thermal energy effects *via* investigated by Hakeem Ullah[26].

The present study is to investigate the combined effects of porous media, Ohmic effect and suction or blowing on 2D radiated viscous nanofluid over unsteady stretching surface. With suitable method the partial differential equation is changed into a system of ordinary differential equations. Numerical solution of resultant equation is obtained by RKF45 technique. The effect of various relevant factors on velocities, concentration, temperature, Nusselt number is determined, and demonstrations are provided through the use of figures and tables.

2.0 Mathematical Description

Consider a boundary layer nanofluid flowing through a porous stretchy material as a result of thermal energy and radiation. The fluid is subsequently electrically transmitted, and the effects of viscosity dissipation, Ohmic, and Joule are not disregarded. Assume that the point of origin is static and the area around it is being extended with velocity U_w (x,t)=ax⁄((1-ct))along x-axis, temperature T_w (x,t)=T_∞+bx⁄((1-ct)), magnetic field B= $B_0/\sqrt{((1-ct)}$) and heat source rate Q= $Q_0/\sqrt{((1-ct)}$). In a direction that is orthogonal to the surface, magnetic field is provided. v_0 is the wall suction /or blowing in

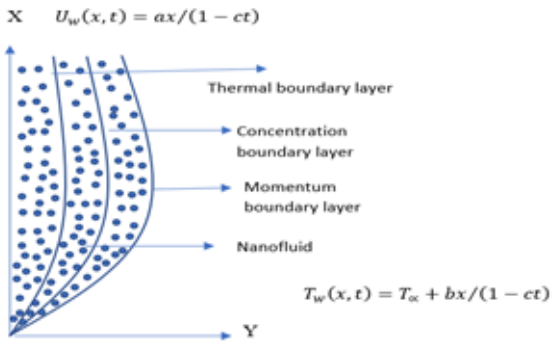


Figure 1. Physical description.

the vertical direction. Figure 1 depicts the geometrical description of the model's physical structure.

Using the assumptions stated above, the equations of movement, energy, and dispersion generated the following result Saleem *et al.*,[27]:

$$\frac{\partial u}{\partial x}+\frac{\partial v}{\partial y}=0 \tag{1}$$

$$\frac{\partial u}{\partial t}+u\frac{\partial u}{\partial x}+v\frac{\partial u}{\partial y}=v\frac{\partial^2 u}{\partial y^2}-\frac{\sigma}{\rho}B^2\mathrm{u}-\frac{v}{K}u \tag{2}$$

$$(\rho c)_f\left(\frac{\partial T}{\partial t}+u\frac{\partial T}{\partial x}+v\frac{\partial T}{\partial y}\right)=k\frac{\partial^2 T}{\partial y^2}+(\rho c)_p\left\{D_B\frac{\partial C}{\partial y}\frac{\partial T}{\partial y}+\frac{D_T}{T_\infty}\left(\frac{\partial T}{\partial y}\right)^2\right\}$$
$$-\frac{1}{\rho C_p}\frac{\partial q_r}{\partial y}+\frac{D_m}{C_\infty}\left(\frac{\partial^2 c}{\partial y^2}\right)+\frac{\mu}{\rho C_p}\left(\frac{\partial u}{\partial y}\right)^2+\frac{Q_0}{\rho C_p}(\mathrm{T}-T_\infty)+\frac{\sigma \mathrm{B_0}^2\mathrm{u}^2}{\rho \mathrm{c_p}} \tag{3}$$

$$\frac{\partial C}{\partial t}+\mathrm{u}\frac{\partial C}{\partial x}+\mathrm{v}\frac{\partial C}{\partial y}=D_B\frac{\partial^2 C}{\partial y^2}+\frac{D_T}{T_\infty}\frac{\partial^2 T}{\partial y^2} \tag{4}$$

Boundary constraints are

$$u(x,0,t)=u_w, v(x,0,t)=v_0, T(x,0,t)=T_W, C(x,0,t)=C_W,$$
$$u(x,\infty,t)=0, T(x,\infty,t)=T_\infty, C(x,\infty,t)=C_\infty \tag{5}$$

Here D_m is mass diffusion coefficient, D_B is Brownian motion, D_T is thermophoretic coefficient, $(\rho c)_p$ is heat capacity of nanoparticle and $(\rho c)_f$ is heat capacity of fluid.

By Rosseland approximation $q_r = -\frac{4\sigma^* \partial T^3}{3k^* \partial y}$ (6)

Expand T^4 using Taylor's series and using (6) we get:

$$(\rho c)_f\left(\frac{\partial T}{\partial t}+u\frac{\partial T}{\partial x}+v\frac{\partial T}{\partial y}\right)=k\left(1+\frac{16\sigma^* {T_\infty}^3}{3k^*}\right)\frac{\partial^2 T}{\partial y^2}+$$
$$(\rho c_p)\left\{D_B\frac{\partial C}{\partial y}\frac{\partial T}{\partial y}+\frac{D_T}{T_\infty}\left(\frac{\partial T}{\partial y}\right)^2\right\}$$
$$+\frac{D_m}{C_\infty}\left(\frac{\partial^2 c}{\partial y^2}\right)+\frac{\mu}{\rho C_p}\left(\frac{\partial u}{\partial y}\right)^2+\frac{Q_0}{\rho C_p}(\mathrm{T}-T_\infty)+\frac{\sigma \mathrm{B_0}^2\mathrm{u}^2}{\rho \mathrm{c_p}} \tag{7}$$

Non-dimensional numbers assumed are

$$(\rho c)_f\left(\frac{\partial T}{\partial t}+u\frac{\partial T}{\partial x}+v\frac{\partial T}{\partial y}\right)=k\left(1+\frac{16\sigma^* {T_\infty}^3}{3k^*}\right)\frac{\partial^2 T}{\partial y^2}+$$
$$(\rho c_p)\left\{D_B\frac{\partial C}{\partial y}\frac{\partial T}{\partial y}+\frac{D_T}{T_\infty}\left(\frac{\partial T}{\partial y}\right)^2\right\}$$
$$+\frac{D_m}{C_\infty}\left(\frac{\partial^2 c}{\partial y^2}\right)+\frac{\mu}{\rho C_p}\left(\frac{\partial u}{\partial y}\right)^2+\frac{Q_0}{\rho C_p}(\mathrm{T}-T_\infty)+\frac{\sigma \mathrm{B_0}^2\mathrm{u}^2}{\rho \mathrm{c_p}} \tag{8}$$

Transformation defined in (8) satisfy equation (1) and equation (2), (4) and (7) takes the form

$$f'''-f'^2+f''f-A\left(\frac{1}{2}\eta f''+f'\right)-(M+\boldsymbol{\lambda})f'=0 \tag{9}$$

$$A\left(\theta+\frac{1}{2}\eta\theta'\right)+f'\theta-f\theta'=\left(\frac{1+R}{P_r}\right)\theta''+ N_b\phi'\theta'+N_t(\theta')^2+\gamma\theta+E_c f''^2+Jf'^2 \tag{10}$$

$$\frac{1}{Sc}\emptyset''-A\,(\eta 2^{-1}\emptyset'+\emptyset)+f'\emptyset-f\emptyset'+\frac{Nt}{Nb}\theta''=0 \tag{11}$$

Dimensionless boundary constraints are:

$$f=S, f'=1, \theta=1, \emptyset=1 \ \ as\ \eta\ tends\ to\ 0$$
$$f'=0, \theta=0, \emptyset=0 \ \ as\ \eta\ tends\ to\ \infty \tag{12}$$

Non dimensional parameters are

$$\mathrm{A}=\frac{c}{a}, =\frac{Q_0}{\rho c_p a}, \ P_r=\frac{\vartheta}{k}, \ \mathrm{M}=\frac{\sigma B_0^2}{\rho a}, \ \mathrm{Ec}=\frac{U_W^2}{C_p\,(T_W-T_\infty)},$$

$$\mathrm{N_b}=\frac{(\rho c)_p}{(\rho c)_f}\frac{D_B}{\vartheta}(\ C_W-C_\infty\ ), \mathrm{N_t}=\frac{(\rho c)_p}{(\rho c)_f}\frac{D_T}{T_\infty \vartheta}(\ T_W-T_\infty\ ),$$

$$\vartheta=\frac{\mu}{\rho}, \ \mathrm{Sc}=\frac{\vartheta}{D_B}, \ \boldsymbol{\lambda}=\frac{v}{K}, \ J=\frac{\sigma \mathrm{H}^2\vartheta}{\rho C_p\,(T_W-T_\infty)}$$

A is Unsteady Parameter, R is Radiation Parameter, M is Magnetic Field field Parameter, P_r is Prandtl Number, Nt is Thermophoresis Constraint, N_b is Brownian Motion Constraint, Ec is Eckert Number, Sc is Schimdt Number, S is the Suction parameter, J is Joule heating effect, λ is permeability parameter.

Skin friction coefficient is given as

$0.5 * C_{fx} \, \mathrm{Re}_x^{\frac{1}{2}} = -f''(0)$, Re denotes the local Reynolds number. (13)

Nusselt number is given as

$$Nu_x \, Re_x^{\frac{-1}{2}} = -\theta'(0) \quad (14)$$

3.0 Numerical Procedure

Since the equations in problem are exceedingly complicated and non-linear, they are challenging to solve mathematically, hence a numerical technique known as the shooting method, followed by the Runge-Kutta technique of fourth order, is utilised with the boundary constraint.

The Runge-Kutta Fehlberg method (RKF45) is one way to tackling this problem. It provides a method for deciding if the proper step size h should be used. At each stage, two unique estimates for the solution are constructed and compared. If two answers are almost identical, an approximation is acceptable.

If the two replies differ to a certain precision, the step size is modified. If the answers agree on an additional set of digits than is required, the step's value increases.

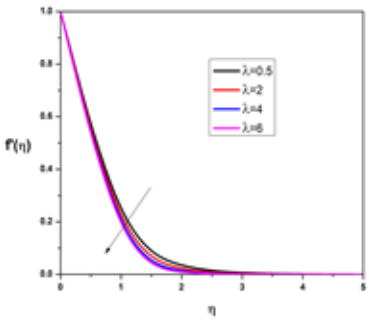


Figure 2. Plot of dimensionless velocity f'(η) verses drag force λ.

The six values indicated below are required for each step size.

$$L_1 = hf(t'_k, y'_k)$$

$$L_2 = hf\left(t'_k + \frac{1}{4}h, y'_k + \frac{1}{4}L_1\right)$$

$$L_3 = hf\left(t'_k + \frac{3}{8}h, y'_k + \frac{3}{32}L_1 + \frac{9}{32}L_2\right)$$

$$L_4 = hf\left(t'_k + \frac{12}{13}h, y'_k + \frac{1932}{2197}L_1 + \frac{7200}{2197}L_2 + \frac{7296}{2197}L_3\right)$$

$$L_5 = hf(t'_k + h, y'_k + \frac{439}{216}L_1 - 8L_2 + \frac{3680}{513}L_3 + \frac{845}{4104}L_4)$$

$$L_6 = hf(t'_k + \frac{1}{2}h, y'_k - \frac{8}{27}L_1 + 2L_2 - \frac{3544}{2565}L_3 + \frac{1859}{4104}L_4 - \frac{11}{40}L_5)$$

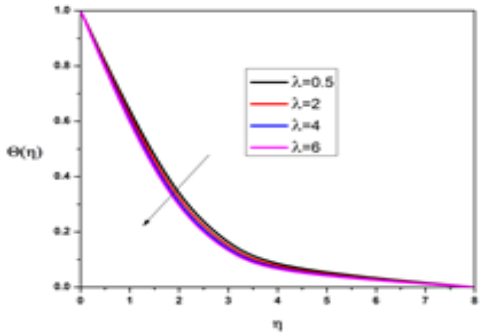


Figure 3. Plot of temperature Θ(η) verses drag force λ.

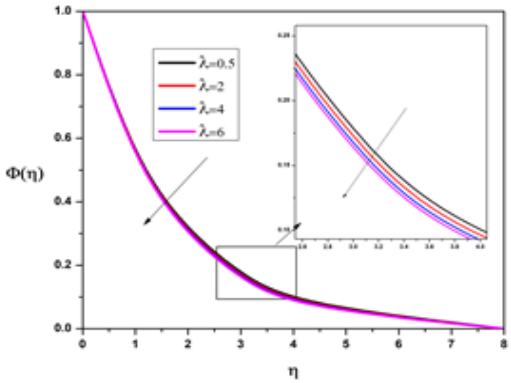


Figure 4. Plot of concentration Θ (η) verses drag force λ .

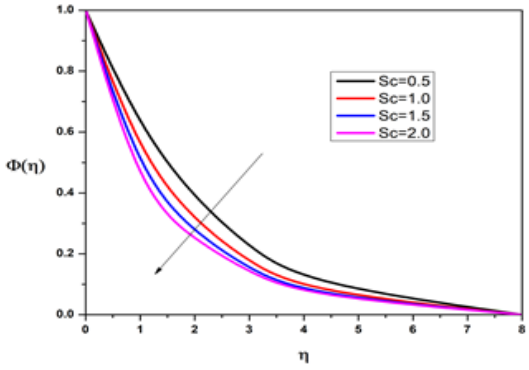


Figure 5. Plot of concentration ϕ(η) verses Schmidt number.

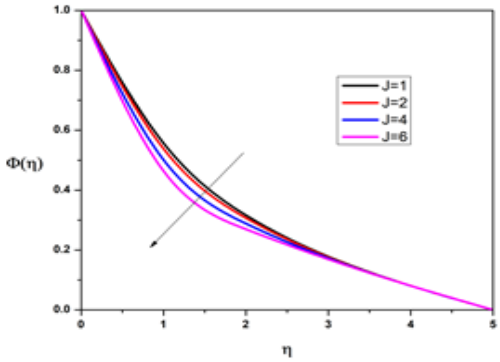


Figure 8. Plot of concentration ϕ(η) verses Joule heating J.

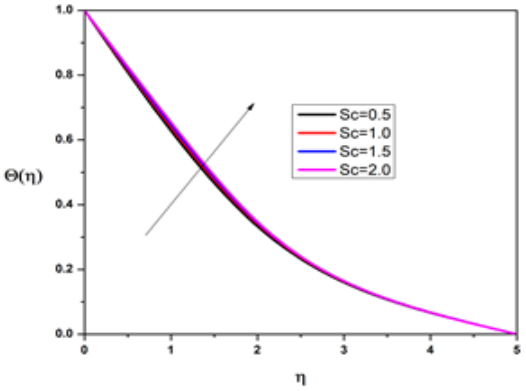


Figure 6. Plot of temperature θ(η) verses Schmidt number.

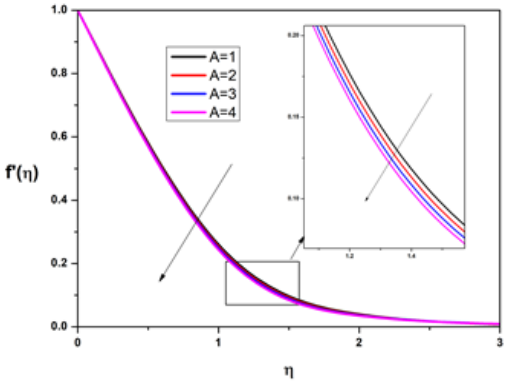


Figure 9. Plot of dimensionless velocity f'(η) verses unsteady parameter A.

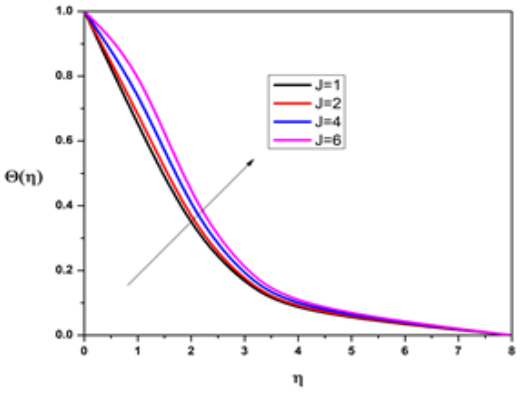


Figure 7. Plot of temperature θ(η) verses Joule heating effect J.

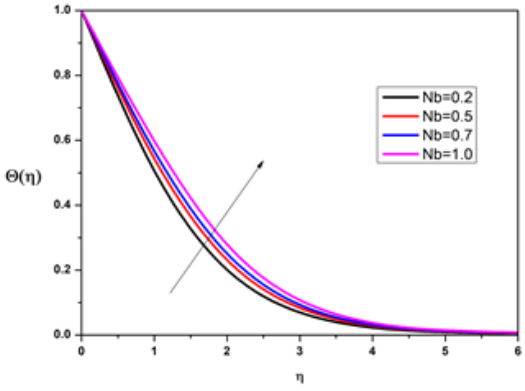


Figure 10. Plot of temperature θ(η) verses Brownian motion constraint N_b.

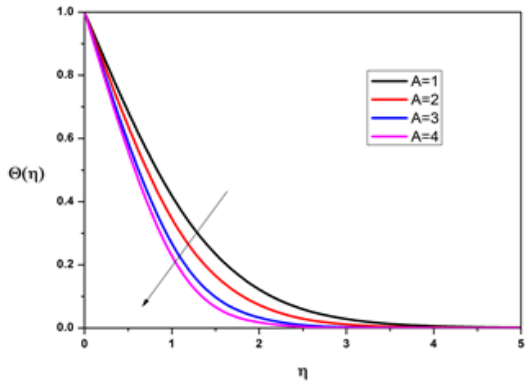


Figure 11. Plot of temperature θ(η) verses unsteady parameter A.

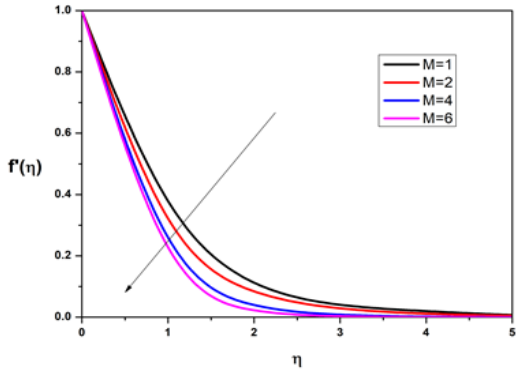


Figure 14. Plot of dimensionless velocity f'(η) verses Hartmann number M.

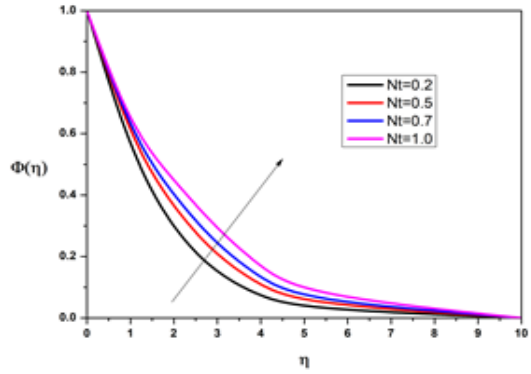


Figure 12. Plot of concentration Φ(η) verses thermophoresis constraint N_t.

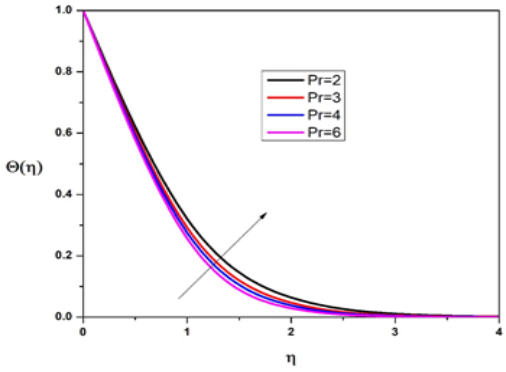


Figure 15. Plot of temperature θ(η) verses Prandtl number Pr.

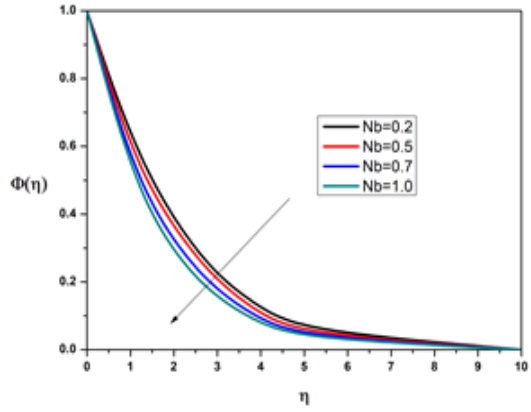


Figure 13. Plot of concentration Φ(η) verses Brownian motion constraint N_b.

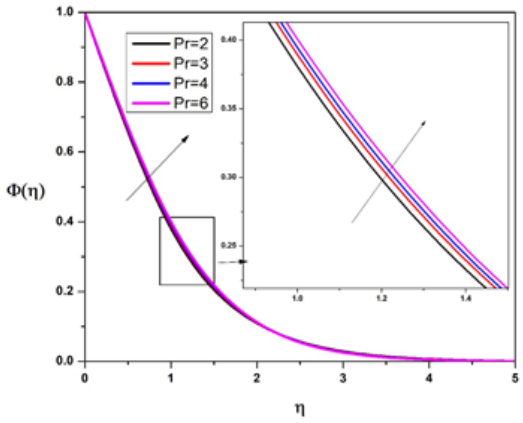


Figure 16. Plot of concentration Φ(η) verses Prandtl number Pr.

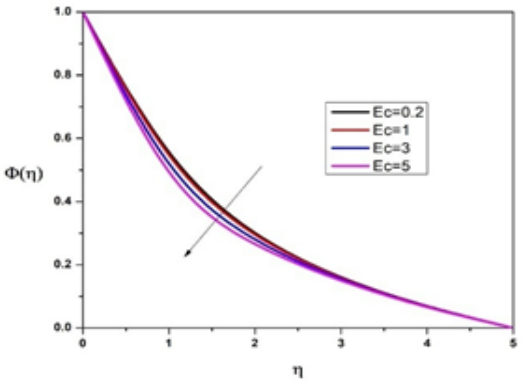


Figure 17. Plot of Concentration Φ(η) verses Eckert number Ec.

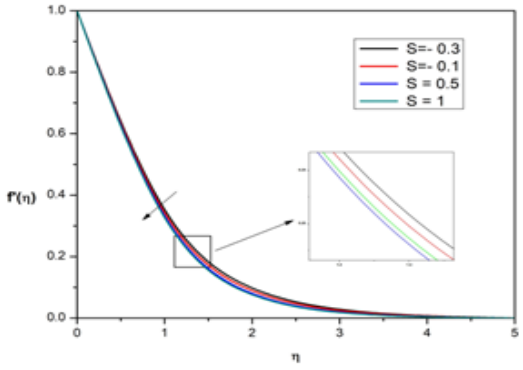


Figure 18. Plot of dimensionless velocity f'(η) verses suction parameter S.

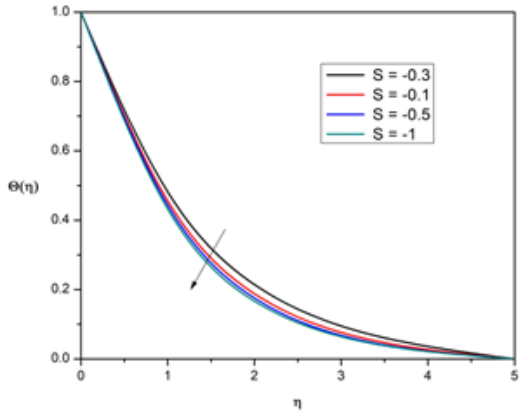


Figure 19. Plot of temperature θ(η) verses suction parameter S.

Then, utilising a Runge-Kutta technique of order 4, a solution to the initial value problem is generated.

$$y'_{k+1} = y'_k + \frac{25}{216}L_1 + \frac{1408}{2565}L_3 + \frac{2197}{4104}L_4 - \frac{1}{5}L_5$$

Figure 2 depicts the effect of the porosity variable on velocities. Because of the lower fluid-particle interaction, velocity has a negative correlation with the permeability value.

Figure 3 depicts the influence of the porosity variable on temperature. When the permeability variable grows, slow motion produces temperature deterioration because the internal temperature of the thermal outermost layer decreases.

Figure 4 shows how the penetration parameter affects concentration. The rising rate for concentration is due to the fact that raising the level of stickiness decreases the flow of fluid, resulting in the quickening of the degree of concentration gradually increasing.

Figure 5 depicts the concentration field value for changing Schmidt number (Sc) values. Figure 5 shows that when Sc levels increase, the fluid's concentration drops. The pace of concentration reduction is quicker at high Sc levels. Because decreased mass diffusivity corresponds to greater values of the Schmidt number. As a consequence, the concentration patterns tend to decrease.

Figure 6 depicts the effect of the Schmidt number Sc on temperature. When the Schmidt number grows, so does the temperature. The Schmidt number quantifies the ratio of diffusivity that heat exhibits to mass diffusion. The higher the Schmidt number, the higher the thermal diffusivity and therefore the temperature profile.

Figure 7 depicts the impact of the Joule heating effect. The graphical data show that while the joule heating increases, the internal temperature of the solution rises, yet the mass density decreases. Figure 8 depicts this, because the joule heat parameter creates warmth in the fluid, as the amount of the joule parameter J grows, the internal temperature of the fluid rises and concentration profiles decline.

The dimensionless velocity f' *vs* parameter A is shown in Figure 9. The velocity falls when the parameter 'A', which represents unsteadiness, is raised. A higher 'A' value, which represents unsteadiness, may cause a temperature drop due to stronger heat transfer effects. Velocity can be lowered by disrupting the fluid's structure and dispersing the energy within the pattern.

Figure 10 depicts the effect of Brownian motion on heat. The inclusion of nanoparticles causes Brownian motion in the nanofluid model, which modifies the fluid's flow rate and heat transfer properties. Brownian motion of nanoscaled nanoparticles enhances fluid flow velocity and hence thermal behaviour.

Figure 11 depicts temperature in relation to parameter A. The temperature decreases while the amount of the parameter 'A', which reflects unsteadiness, is increased. A higher 'A' value, which represents unsteadiness, may cause a temperature drop due to stronger heat transfer effects.

Figures 12 and 13 depict the effects of Nb and Nt on intensity trends for different parameter values, culminating in the expansion of the small particles border concentration layer. Brownian motion demonstrates reversal behaviour at the nanoscale fluid concentration boundary layer. Both friction coefficient values are found to grow as the fraction of nanoparticle volume rises. while a result, if the value of Nb rises, so does the concentration. Nt appears to have an influence on raising nanofluid concentration at higher values of the specified parameter.

The velocity variations as a result of the parameter magnetic are depicted in Figure 14. The presence of a magnetic field creates electricity throughout the flow of the fluid domain, which provides opposition, allowing the fluid's temperature increase and its speed to decrease due to the Lorentz force.

Figure 15 depicts the effect of the Prandtl number on flow temperature. According to the graph, as Pr grows, so do the temperatures fields. Based on the physics of the Prandntl number, the measured trend in the fluid's warmth is accurate. By linking the viscosity of kinematics to thermal diffusivity, the Prandtl number connects the velocity of the boundary layer to the velocity of the radiative boundary layer. The lower the Prandtl value, higher the thermal diffusivity.

Figure 16 depicts the effect of the Prandtl number on flow concentration. According to the graph, as Pr grows, so do the intensity of fields.

Figure 17 depicts the fluctuation in Eckert number with intensity. Concentration suffers when the Eckert number rises. This is due to the inclusion of the viscosity effects Ec, which raises the temperature of the fluid, which converts mechanical energy to thermal energy. The fluid thins as a result, boosting velocity while lowering mass concentration.

Figures 18 and 19 depict the effect of the suction variable S on the velocity distribution and thermal boundary region layer. The increasing suction parameter S is seen, where the flow rate of the fluid is shown to rise with blowing. Whenever external suction (S>0) is taken into account, the dimensionless velocities field decreases and the outer edges of the layer's thickness decrease.

Table 1 compares the skin coefficients of friction obtained for different values of Pr, A, M, and R in the absence of nanofluid to Saleem *et al.,* and Ishak[28]. The Nusselt number is compared in Table 2 for different amounts of Pr, Sc, Ec, and R. It also displays the current results for J, S, and λ. The result is relevant to the current work.

Table 1. The skin friction coefficients for a number of parameters

Pr	A	M	R	Ishak[28]	Saleem *et al.*[27]	Present Result
0.72	0	0	0	0.8086	0.80861	0.808612
1				1	1.00024	1.000241
3				1.9237	1.92361	1.923611
0.72	1	1	1	NA	0.70864	0.708642
1				NA	0.8678	0.86782
3				NA	1.6081	1.60814

Table 2. The Heat transfer rate coefficient for a number of parameters

Sc	Pr	Ec		R		J	S	Nusselt no. Saleem *et al.*[27]	Nusselt no. (Present)	Sherwood numberSaleem *et al.*[27]	Sherwood number (Present)
0.5								0.14731	0.147311	0.20656	0.206566
1								0.14986	0.149863	-0.03305	-0.033051
1.5								0.1511	0.15112	-0.13568	-0.135685
	4							-0.68762	-0.687623	0.67507	0.675074
	8							-0.26558	-0.265581	1.04382	1.043822
	12							2.25205	2.252053	1.15988	1.15988
		0.5						-0.04382	-0.043822	0.22857	0.228573
		1						0.0859	0.08591	0.28849	0.288496
		1.5						0.21567	0.215674	0.34841	0.348414
			0.1					0.14757	0.147571	0.18064	0.180643
			0.2					0.10086	0.100863	0.19703	0.197032
			0.3					0.05304	0.053041	0.21353	0.213533
				0.5				0.11933	0.119335	0.22857	0.228571
				1				0.11035	0.110351	0.28849	0.288492
				1.5				0.09219	0.092196	0.34841	0.348413
					0.2			-	0.204575	-	0.354456
					0.4			-	0.200013	-	0.345568
					0.6			-	0.199355	-	0.333444
						0.1		-	0.251436	-	0.294578
						0.3		-	0.264587	-	0.306579
						0.5		-	0.273465	-	0.299945
							0.1	-	1.105448	-	0.226458
							0.2	-	1.000456	-	0.215487
							0.3	-	0.995454	-	0.201254

4.0 Conclusions

The influence of magnetohydrodynamic convection unsteady flow as well as heat transmission across an environment in the presence of pemiability, suction or blowing, viscous dissipation, and the joule heating effect was explored. The equations governing the problem are solved numerically using the RKF45 Runge-Kutta Felhberg Method. The graphs show the impacts of various factors on flow and heat transmission, which are outlined as follows:

- Velocity profile decreases with enhancement in magnetic parameter λ, *M*, A and S parameter since the flow is retarded by these parameters.
- Thermal boundary layer grows with Nb, Ec, Pr, J and Sc parameter while shows opposite behaviour with S, λ, and A parameter.
- Heat trasfer rate increases under the influence of J while it decline with λ and Su.
- Improvement in concentration profile is visible for Pr and Nt parameter but reverse trend is observed with A, Ec, Nb, J, and Sc parameter.
- The study sheds light on the migration of viscous nanomaterials like metals (Al, Au, Cu, Fe, Ag), metal oxide (Al_2O_3, TiO_2, CuO), layered (Al+ Al_2O_3, Cu+C), carbon materials (graphite, CNTs, diamond) and nitride (AlN, SiN).

5.0 References

1. Sakiadis BC. Boundary-layer behavior on continuous solid surfaces: II. The boundary layer on a continuous flat surface. AIChE J. 1961; 7(2):221–5. https://doi.org/10.1002/aic.690070211
2. Crane LJ. Flow past a stretching plate. Zeitschrift fur Angew Math und Phys ZAMP. 1970; 21(4):645–7. https://doi.org/10.1007/bf01587695
3. Choi SUS, Eastman JA. Enhancing thermal conductivity of fluids with nanoparticles. Am Soc Mech Eng Fluids Eng Div FED. 1995; 231:99–105.
4. Buongiorno J. Convective transport in nanofluids. J Heat Transfer. 2006; 128(3):240–50. https://doi.org/10.1115/1.2150834
5. Eid MR, Mabood F. Two-phase permeable non-Newtonian cross-nanomaterial flow with Arrhenius energy and entropy generation: Darcy-Forchheimer model. Phys Scr. 2020; 95(10):105209. https://doi.org/10.1088/1402-4896/abb5c7
6. Gireesha BJ, Mahanthesh B, Manjunatha PT, Gorla RSR. Numerical solution for hydromagnetic boundary layer flow and heat transfer past a stretching surface embedded in non-Darcy porous medium with fluid-particle suspension. J Niger Math Soc. 2015; 34(3):267–85. https://doi.org/10.1016/j.jnnms.2015.07.003
7. Hosseinzadeh K, Gholinia M, Jafari B, Ghanbarpour A, Olfian H, Ganji DD. Nonlinear thermal radiation and chemical reaction effects on Maxwell fluid flow with convectively heated plate in a porous medium. Heat Transf Res. 2019; 48(2):744–59. https://doi.org/10.1002/htj.21404
8. Makinde OD, Chinyoka T. MHD transient flows and heat transfer of dusty fluid in a channel with variable physical properties and Navier slip condition. Comput Math Appl. 2010; 60(3):660–9. https://doi.org/10.1016/j.camwa.2010.05.014
9. Hayat T, Aziz A, Muhammad T, Alsaedi A. Darcy–Forchheimer three-dimensional flow of Williamson nanofluid over a convectively heated nonlinear stretching surface. Commun Theor Phys. 2017; 68(3):387. https://doi.org/10.1088/0253-6102/68/3/387
10. Rasool G, Shafiq A, Baleanu D. Consequences of Soret–Dufour effects, thermal radiation, and binary chemical reaction on Darcy Forchheimer flow of nanofluids. Symmetry. 2020; 12(9):1421. https://www.mdpi.com/2073-8994/12/9/1421
11. Venkatadri K, Gaffar SA, Babu CS, Fazuruddin S. MHD radiative heat transfer analysis of Carreau nanofluid flow past over a vertical plate: A numerical study. Nanosci Technol Int J. 2021; 12(4):81–103. https://doi.org/10.1615/nanoscitechnolintj.202103565912.
12. Khan WA, Pop I. Boundary-layer flow of a nanofluid past a stretching sheet. Int J Heat Mass Transf. 2010; 53(11–12):2477–83. https://doi.org/10.1016/j.ijheatmasstransfer.2010.01.032
13. Makinde OD, Aziz A. Boundary layer flow of a nanofluid past a stretching sheet with a convective boundary condition. Int J Therm Sci. 2011; 50(7):1326–32. https://doi.org/10.1016/j.ijthermalsci.2011.02.019
14. Cortell R. Viscous flow and heat transfer over a nonlinearly stretching sheet. Appl Math Comput. 2007; 184(2):864–73. https://doi.org/10.1016/j.amc.2006.06.077
15. Prasad KV, Santhi SR, Datti PS. Non-Newtonian power-law fluid flow and heat transfer over a non-linearly

stretching surface. Appl Math. 2012; 03(05):425–35. https://doi.org/10.4236/am.2012.35065
16. Mukhopadhyay S, Ranjan De P, Layek GC. Heat transfer characteristics for the Maxwell fluid flow past an unsteady stretching permeable surface embedded in a porous medium with thermal radiation. J Appl Mech Tech Phys. 2013 6; 54(3):385–96. https://doi.org/10.1134/s0021894413030061
17. Srinvasulu T, Bandari S. MHD boundary layer flow of nanofluid over a nonlinear stretching sheet with effect of non-uniform heat source and chemical reaction. J Nanofluids. 2017; 6(4):637–46. https://doi.org/10.1166/jon.2017.1362
18. Jafar AB, Shafie S, Ullah I. MHD radiative nanofluid flow induced by a nonlinear stretching sheet in a porous medium. Heliyon. 2020; 6(6):e04201. https://doi.org/10.1016/j.heliyon.2020.e04201
19. Elgazery NS. Nanofluids flow over a permeable unsteady stretching surface with non-uniform heat source or sink in the presence of inclined magnetic field. J Egypt Math Soc. 2019; 27(1):9. https://doi.org/10.1186/s42787-019-0002-4
20. Jafar AB, Shafie S, Ullah I, Safdar R, Jamshed W, Pasha AA, *et al*. Mixed convection flow of an electrically conducting viscoelastic fluid past a vertical nonlinearly stretching sheet. Sci Rep. 2022; 12(1):14679. https://doi.org/10.1038/s41598-022-18761-0
21. Saeed A, Alghamdi W, Mukhtar S, Shah SIA, Kumam P, Gul T, *et al*. Darcy-Forchheimer hybrid nanofluid flow over a stretching curved surface with heat and mass transfer. Plos One. 2021; 16(5):e0249434. https://doi.org/10.1371/journal.pone.0249434
22. Abbas N, Rehman KU, Shatanawi W, Malik MY. Numerical study of heat transfer in hybrid nanofluid flow over permeable nonlinear stretching curved surface with thermal slip. Int Commun Heat Mass Transf. 2022; 135:106107. https://doi.org/10.1016/j.icheatmasstransfer.2022.106107
23. Jue TC. Analysis of thermal convection in a fluid-saturated porous cavity with internal heat generation. Heat Mass Transf. 2003; 40(1–2):83–9. https://doi.org/10.1007/s00231-003-0420-5
24. Pavel BI, Mohamad AA. An experimental and numerical study on heat transfer enhancement for gas heat exchangers fitted with porous media. Int J Heat Mass Transf. 2004; 47(23):4939–52. https://doi.org/10.1016/j.ijheatmasstransfer.2004.06.014
25. Reddy KV, Reddy MG, Reddy GR, Makinde OD. Analysis of joule heating and chemical reaction effects in electroosmosis peristaltic transport of couple-stress, micropolar and nanofluids. J Nanofluids. 2023; 12(3):796–808. https://doi.org/10.1166/jon.2023.1963
26. Ullah H, Fiza M, Khan K, Batool S, Ghufran SM, Al-Mekhlafi SM. Effect of joule heating and thermal radiation of MHD boundary layer Oldroyd-B nanofluid flow with heat transfer over a porous stretching sheet by finite element method. J Nanomater. 2022: pp. 1–11. https://doi.org/10.1155/2022/7373631
27. Saleem S, Nadeem S, Rashidi MM, Raju CSK. An optimal analysis of radiated nanomaterial flow with viscous dissipation and heat source. Microsyst Technol. 2019; 25(2):683–9. https://doi.org/10.1007/s00542-018-3996-x
28. Ishak A. Unsteady MHD flow and heat transfer over a stretching plate. J Appl Sci. 2010; 10(18):2127–31. https://doi.org/10.3923/jas.2010.2127.2131